Iranica Journal of Energy & Environment
Journal Homepage: www.ijee.net
IJEE an official peer review journal of Babol Noshirvani University of Technology, ISSN:2079-2115

Effect of Mn Doping on Fe_3O_4 Nanoparticles Synthesized by Wet chemical Reduction Technique

T. J. Malek[1]*, S. H. Chaki[1], M. D. Chaudhary[1], J. P. Tailor[2] and M. P. Deshpande[1]

[1]*P. G. Department of Physics, Sardar Patel University, Vallabh Vidyanagar – 388120, Gujarat, India*
[2]*Applied Physics Department, S.V.N.I.T., Surat – 395007, Gujarat, India*

P A P E R I N F O

Paper history:
Received 30 May 2018
Accepted in revised form 10 july 2018

Keywords:
Fe3O4
Nanoparticles
Wet chemical reduction
Surface morphology
Magnetic properties

A B S T R A C T

The effect of Mn doping on Fe_3O_4 nanocrystalline spinel particles is studied. Two doping concentrations of 10 and 15% Mn were employed. The nanoparticles synthesis was carried out by wet chemical reduction technique. The energy dispersive analysis of X-ray confirmed the stoichiometry of the samples. The X-ray diffraction technique was used to determine the crystal structure and particles size of the synthesized nanoparticles. The electron microscopy revealed that both the synthesized nanoparticles surfaces have flower-like patterns and the particles are spherical. The optical absorption study showed that the absorption is more in case of 10% Mn doped compared to 15% Mn doped Fe_3O_4 nanoparticles. The Fourier transform infra-red spectroscopy revealed that both the samples contain characteristics bands. The magnetization variation with temperature with zero field cooled and field cooling conditions for two different applied magnetic fields of 500 Oe and 1000 Oe as well as the hysteresis study was carried out by vibrating sample magnetometer technique. The obtained results are discussed in details.

***doi**: 10.5829/ijee.2018.09.02.07*

INTRODUCTION

In recent time, interests in room-temperature magnetic nanostructures have been steadily increasing because of their potential applications in data recording and spintronic devices [1]. Iron oxides possess many advantages in technological applications, due to their exclusive combination of magnetic and electrical properties. One of the important iron oxides, magnetite (^c Fe3o4), is known to undergo a ferrimagnetic transition at a Curie temperature (TC) of ~850 K [2]. It has an inverse spinel structure, symbolized as [Fe3+]A[Fe2+Fe3+]BO4, in which the A-sites (tetrahedral sites) are occupied by the Fe3+ ions and the B-sites (octahedral sites) by equal numbers of Fe2+ and Fe3+ ions. A possible explanation for the observed ferrimagnetism in Fe_3O_4 is the double exchange interaction through Fe2+ and Fe3+ ions at the B-sites, while the A- and B-site spins are antiferromagnetically (AF) coupled. At room temperature, the high electronic conductivity of Fe_3O_4 is due to rapid electron hopping between Fe2+ and Fe3+ ions occupying the B-sites. Furthermore, Fe_3O_4 undergoes a first-order metal-insulator phase transition at TV = 120-130 K (Verwey temperature), where long-range charge ordering of the Fe2+ and Fe3+ ions in the B-site sub-lattices occur [3].
In the last few decades due to the emphasis on miniaturization, Fe_3O_4 has been studied in low-dimensional nanostructure forms [4-8]. The current biological applications of Fe_3O_4 in nanoforms are quantum dots (QDs) for targeted drug delivery, as ultrasensitive bio-agent detector, in gene therapy, in hydro thermic cancer treatment, in magnetic resonance imaging (MRI) contrast enhancement, magnetic bio-sensing, thermal ablation and ferromagnetic resonance [8-12].

The application range of magnetite can be extended by varying their properties by substituting iron atoms by other transition metal ions. Literature shows magnetite has been doped by transition metal ions like Mn2+, Zn2+, Ni2+ and Co2+ [13, 14]. These studies revealed that doped Mn2+ and Zn2+ ions showed preference to occupy the A-sites, while Ni2+ and Co2+ ions tend to occupy the octahedral B-sites in the inverse spinel structure [13, 14]. It has been reported that 17% Mn doping in Fe_3O_4 films, decreases the carrier concentration without affecting the electron mobility, but increases their spin polarization, thus stating the substitution of Mn ions at the tetrahedral (Td) sites [14]. Whereas Co doped Fe_3O_4 films showed increased magnetic anisotropy stating that Co2+ ions occupy the octahedral (Oh) sites [15]. Doped iron oxides have been found to be gas sensors [16, 17]. Sensing to the significance of doping in Fe_3O_4 and apprehending the materials interest in fundamental science and application in various nanodevices, the authors got interested to study the effect of transition metal doping on the properties of

* Corresponding author: Tasmira J. Malek
E-mail: tasmirasybsc02@yahoo.co.in

Fe_3O_4 nanostructures. Various techniques to synthesis magnetite nanocrystals have been reported, including sol–gel [18], co-precipitation [19], reverse micelles [20], hydrothermal [21], autocombustion [22] and sonochemical reaction [23].

In this study, the authors synthesized Mn doped Fe_3O_4 nanoparticles by wet chemical reduction technique. The reason for selecting wet chemical technique was its simplicity and synthesis at room condition. Two doping concentrations of 10 and 15% Mn were employed in doping the Fe_3O_4 nanoparticles. The present work provides insights into the structural, optical and magnetic properties of the two different Mn doping concentrations in Fe_3O_4 nanoparticles.

MATERIAL AND METHODS

Synthesis of Mn doped Fe_3O_4 nanoparticles

Wet chemical technique was employed to synthesis Mn doped Fe_3O_4 nanoparticles. The synthesis was done by taking 10 ml of 2.5M sodium boro-hydride (NaBH4; Sisco Chem, Mumbai, India) solution in a 100 ml dry clean glass beaker. To it is added 40 ml of 0.12M ferric chloride hexa-hydrate (FeCl3•6H2O; Loba Chemie, Mumbai, India) solution under constant stirring. Subsequently, after 10 min. of vigorous stirring, 10 ml of 0.18M and 0.20M manganese chloride tetra-hydrate (MnCl2•4H2O; Chiti-chem., Vadodara, India) was added to the solution to get 10 and 15% Mn doped Fe_3O_4 nanoparticles, respectively. The above chemical proportion selection for synthesis was accomplished by trial and error method. The solution addition was done drop wise under constant vigorous stirring. It was observed that with gradual addition, the final solution became darker and eventually became black. After complete addition, black precipitates were formed in the solution in less than 1 min. The above chemical reaction produces magnetite nanoparticles, boro-hydroxide, sodium chloride and hydrogen gas. The occurrence of reaction leading to the production of nanoparticles in the beaker was made sure by the generation of bubbles due to hydrogen gas and the reaction was considered to be over once bubble formation ceases. The synthesized Mn doped Fe_3O_4 nanoparticles were given multiple washes with de-ionized water and dried overnight at 40□C in an oven.

Characterization

The elemental analyses of the as-synthesized nanoparticles were made by energy dispersive analysis of X-ray (EDAX) technique attached to Philips XL 30 ESEM scanning electron microscope. The structural analysis of the nanoparticles were done by recording powder X-ray diffraction (XRD) patterns using Philips X'Pert MPD X-ray diffractometer employing graphite monochromatized CuKα radiation (λ = 1.5405Å). The particle size study of the nanoparticles was done using transmission electron microscopy (TEM) employing JEOL, JEM-2100. The morphology study was carried out using scanning electron microscopy (SEM) employing SEM LEO 1430 VP. The optical absorption spectrum was recorded using Perkin-Elmer Lambda-19 spectrophotometer. The Fourier transform infrared spectroscopy (FTIR) study of the as-synthesized nanoparticles was done employing Perkin-Elmer Spectrum GX spectrometer. The magnetic properties of the nanoparticles were studied employing the Quantum design, 14T PPMS vibrating sample magnetometer (VSM).

RESULTS AND DISCUSSION

Chemical characterizations

Energy dispersive analysis of X-ray (EDAX) The observed EDAX spectrum for both the samples is shown in Figure 1(a, b). The EDAX data of weight % of the elements observed in the as-synthesized 10 and 15% Mn doped Fe_3O_4 nanoparticles are tabulated in Table 1. The corresponding standard weight % data is also given in Table 1. The observed weight % data are in good agreement with the standard data. The EDAX analysis also confirms that the samples have only Mn, Fe and O elements thus they do not possess any impurities.

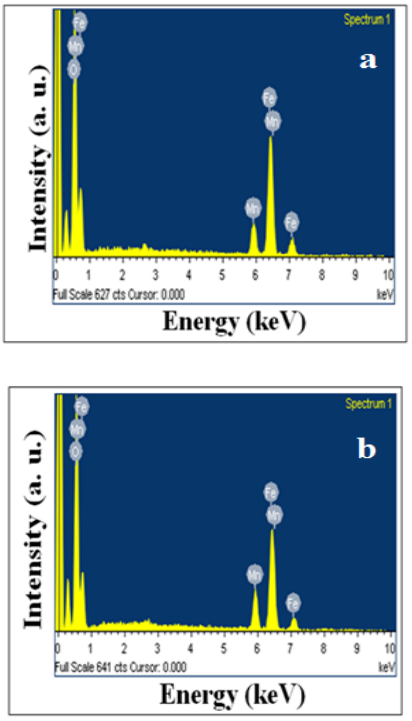

Figure 1. The EDAX spectrum of as-synthesized (a) 10% and (b) 15% Mn doped Fe_3O_4 nanoparticles

TABLE 1. The EDAX data of 10% and 15% Mn doped Fe_3O_4 nanoparticles

Elements	10% Mn doped Fe_3O_4 nanoparticles		15% Mn doped Fe_3O_4 nanoparticles	
	Observed Wt%	Standard Wt%	Observed Wt%	Standard Wt %
Fe	58.97(1)	59.51	55.89(1)	56.54
O	32.49(1)	33.15	32.11(1)	32.41
Mn	8.54(1)	7.34	12.00(1)	11.05

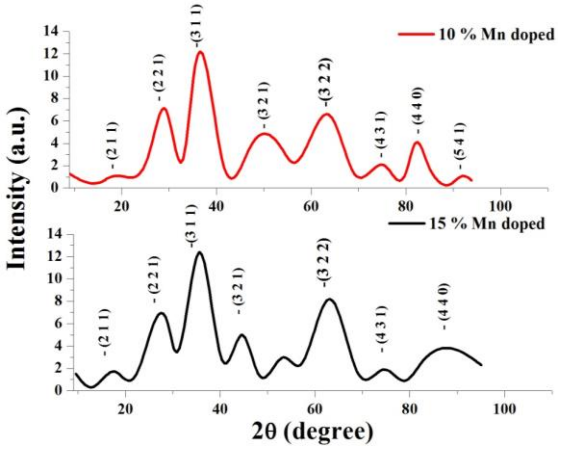

Figure 2. The XRD patterns of as-synthesized 10% and 15% Mn doped Fe_3O_4 nanoparticles

Structural characterizations

X-ray diffraction (XRD) The X-ray diffraction (XRD) patterns of the as-synthesized 10 and 15% Mn doped Fe_3O_4 nanoparticles are shown in Figure 2. The diffraction peaks could be indexed as those of cubic structure of Fe_3O_4 phase having lattice parameter a as 8.365 and 8.368Å for 10% Mn and 15% Mn doped Fe_3O_4 nanoparticles, respectively. The determined lattice parameters are in agreement with the standard inverse cubic spinel phase of iron oxide, a = 8.39 Å (JCPDS: 01-88-0315) [24]. The XRD shows that the major peaks in both the patterns are identical regardless of Mn content. Only one weak peak around 53 in 15% Mn doped Fe_3O_4 nanoparticles could not be indexed. This un-indexed peak may be due to incommensurate modulation of the basic structure due to larger amount of 15% doping by Mn. There is no evidence of peaks corresponding to manganese oxide (MnO2 or Mn3O4) confirming that the doped Mn is incorporated into the ferrite structure as a substitute rather than precipitating as a manganese oxide. The broadening of the experimental peaks suggests the occurrence of nanocrystalline domains within the Mn doped iron oxide clusters. The minute analysis of XRD patterns shows that there is shift in peaks due to variation in the doping concentration of Mn dopant. The shift in the XRD peaks of doped materials arises due to dopants as per the Vegard's law. The law states that the dopant does not produce its own peak, but produces adequate shift in the position of host peak [25]. This observation clearly affirms that in the process of doping of Fe_3O_4, the Mn dopants replace Fe ions.

The below mentioned Scherrer's equation was employed to determine the crystallite sizes using the XRD data [26],

$$D = \frac{k\lambda}{\beta\cos\theta} \qquad (1)$$

where D is crystallite size, k is the grain shape factor taken as unity since the particles are spherical in shape as observed in the TEM images discussed later in the manuscript (Section 3.3.2), λ is the incident X-ray wavelength of CuKα radiation and θ is the Bragg's angle, β is the broadening of diffraction lines measured in radians at half maximum intensity. The determined crystallite sizes came out as 7.15(1) nm and 7.89(1) nm for 10 and 15% Mn doped Fe_3O_4 nanoparticles, respectively.

Similar to above crystallite size determination, the Hall – Williamson (H-W) relation [26] was employed to determine the crystallite sizes and the micro strains of the as-synthesized 10 and 15% Mn doped Fe_3O_4 nanoparticles using the XRD data.

$$\frac{\beta\cos\theta}{\lambda} = \frac{k}{D} + \frac{4\varepsilon\sin\theta}{\lambda} \qquad (2)$$

The H-W equation consists of Scherrer's formula of crystallite size and the micro strain term. Here β is full width at half maximum (FWHMs) of the diffraction peaks, which is expressed as a linear combination of the contributions from the strain (ε) and crystallite size (D). The plot of 4sinθ/ λ verses βcosθ/λ is a straight line, Figure 3, in which the reciprocal of the intercept on βcosθ/λ axis gives the average crystallite size and the slope gives the residual strain. The crystallite sizes determined from the intercept comes out to be ~ 6.89 nm and 7.65 nm for 10 and 15% Mn doped Fe_3O_4 nanoparticles, respectively. The respective crystallite sizes determined by H-W relation are in agreement with the respective crystallite sizes determined by Scherrer's equation. The residual strain values determined from the slopes of the plots came out to be +3.51 x 10-3 and +5.85 x 10-3 for the as-synthesized 10 and 15% Mn doped Fe_3O_4 nanoparticles, respectively. The positive values of the residual strains for the Mn doped Fe_3O_4 nanoparticles indicates it to be tensile strains.

Morphological analysis

Scanning Electron Microscopy The SEM images of as-synthesized 10% Mn doped Fe_3O_4 nanoparticles are shown in Figure 4 (a, b and c), whereas of 15% Mn doped Fe_3O_4 nanoparticles are shown in Figure 4 (d, e and f). The SEM images of both, 10 and 15% Mn doped Fe_3O_4 nanoparticles; clearly show that the nanoparticles surfaces are covered by flower-like patterns. The magnified SEM images show that the flower-like pattern is formed by the cluster of several nano-sheets.

Transmission Electron Microscopy The TEM images of the as-synthesized 10 and 15% Mn doped Fe_3O_4 nanoparticles are shown in Figure 5. The samples for TEM observations were prepared by dispersing the particles in de-ionized water under sonication of 30 min., then placing a drop of the dispersion onto a copper grid with a layer of amorphous carbon. The Figure 5(a, b) shows the TEM images of 10% and Figure 5(c, d) shows the TEM images of 15% Mn doped Fe_3O_4 nanoparticles at different magnifications. The images clearly reveal that the particles are spherical in shape. The images also states that the spheres are of varied dimensions.

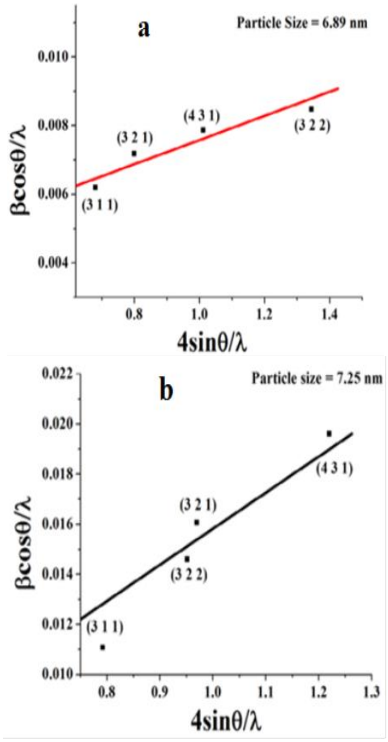

Figure 3. The Hall-Williamson plots for synthesized (a) 10% and (b) 15% Mn doped Fe_3O_4 nanoparticles

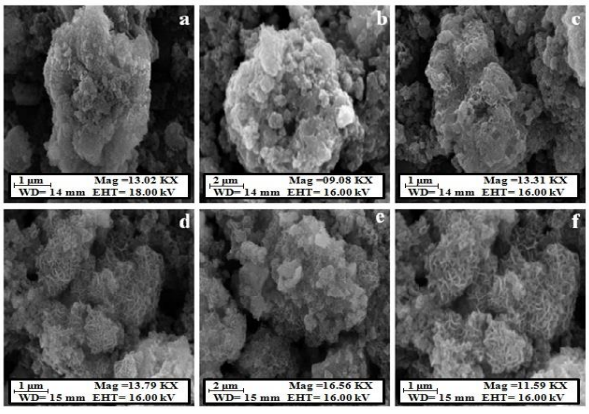

Figure 4. The SEM images of the as-synthesized (a, b, c) 10% and (d, e, f) 15%Mn doped Fe_3O_4 nanoparticles

Optical study

UV–Vis - NIR analysis The Figure 6 shows the optical absorbance spectra of the as-synthesized 10 and 15% Mn doped Fe_3O_4 nanoparticles at ambient temperature. The clear colloid obtained after 30 minute sonication of as-synthesized 10 and 15% Mn doped Fe_3O_4 nanoparticles dispersed in de-ionized water were taken as samples and pure de-ionized water was used as reference. The spectra show that the absorbance edges lie in the range of 210 nm and 235 nm wavelength for both the samples. Above 235 nm wavelength, the absorption increases till nearly 400 nm wavelength and after that it becomes near stable till 700 nm. The spectra show that the absorption is more in case of 15% Mn doped Fe_3O_4 nanoparticles compared to 10% Mn doped Fe_3O_4 nanoparticles in the wavelength range above λ235 nm. This may be due to larger crystallite size in case of 15% Mn doped Fe_3O_4 nanoparticles compared to 10% Mn doped Fe_3O_4 nanoparticles as observed in the XRD analysis.

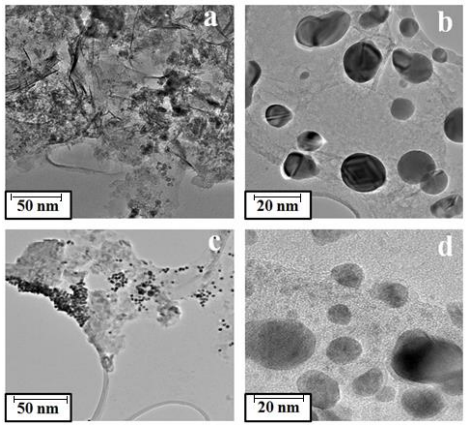

Figure 5. TEM images of the synthesized (a, b) 10% and (c, d) 15% Mn doped Fe_3O_4 nanoparticles

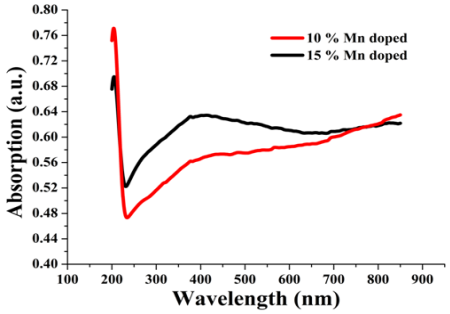

Figure 6. Optical absorbance spectra of as-synthesized 10% and 15% Mn doped Fe_3O_4 nanoparticles at ambient temperature

Fourier Transform Infrared Spectroscopy (FTIR)
The FTIR spectra of dispersed as-synthesized 10% and 15% Mn doped Fe_3O_4 nanoparticles in de-ionized water are shown in Figure 7. The peaks at 3418.72 cm-1 and 3413.17 cm-1 are due to the O-H stretching vibration arising from the hydroxyl groups of the water on the nanoparticles [27]. The absorption peaks at 2954.91 cm-1, 2925.79 cm-1, 2922.13 cm-1, 2852.45 cm-1, 1627.50 cm-1, 1597.44 cm-1 and 1560.66 cm-1 are due to de-ionized water used as solvent [28]. The bands at 1491.18 cm-1 and 1349.66 cm-1 corresponds to the characteristic stretching frequencies of the carboxyl [29]. The broad absorption peaks of 1023.24 cm-1, 927.20 cm -1 in 10% Mn doped Fe_3O_4 and 1024.30 cm-1, 869.98 cm-1 in 15% Mn doped Fe_3O_4 are due to the bonded hydroxyl groups on the metal of the oxide surface [30]. The peaks at 684.03 cm-1, 590.03 cm-1 of 10% Mn and 693.33 cm-1 of 15% Mn doped Fe_3O_4 nanoparticles are assigned to the Fe-O bond [31]. The characteristic peaks of 507.27 cm-1 and 503.69 cm-1 are attributed to Mn-O bond for the 10 and 15% Mn doped Fe_3O_4 [32] nanoparticles, respectively. The FTIR spectra confirm the participation of carboxyl, hydroxyl, Fe–O, and Mn–O groups in the adsorption process. The presence of Mn-O bond substantiates doping of Mn into the spinel Fe_3O_4 structure.

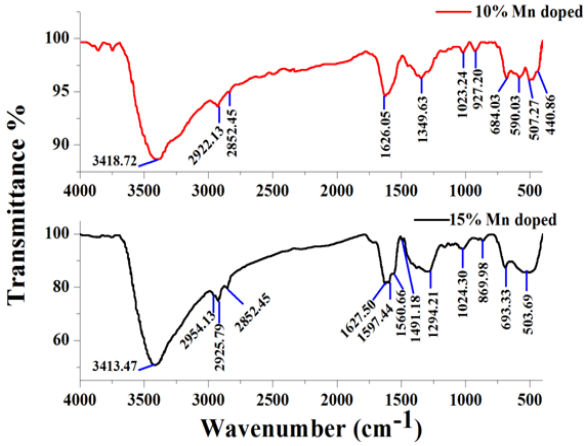

Figure 7. The FTIR spectra of the as-synthesized 10% and15% Mn doped Fe_3O_4 nanoparticles at ambient temperature

Magnetic study
Vibrating Sample Magnetometer (VSM) The variation of sample magnetization as a function of temperature with zero field cooled (ZFC) and field cooling (FC) conditions for the as-synthesized 10 and 15% Mn doped Fe_3O_4 nanoparticles are shown in Figure 8 for two different applied magnetic fields of 1000 Oe and 500 Oe. The temperature variation was from 4K to 320K. It is observed that for applied magnetic field of 1000 Oe, the magnitude of variation of sample magnetization in case of 15% Mn doped Fe_3O_4 nanoparticles are more compared to 10% Mn doped Fe_3O_4 nanoparticles. The large crystallite size observed from the XRD analysis in case of 15% Mn doped Fe_3O_4 nanoparticles compared to 10% Mn doped Fe_3O_4 nanoparticles is responsible for the large variation of magnetization with temperature for applied magnetic field of 1000 Oe. The larger crystallite size is closer to the single magnetic domain, which leads to an easy turn of magnetic moments and facile magnetization [33]. While in case of 500 Oe applied magnetic field, the variation of sample magnetization with temperature is negligible for both the doping concentrations. This may be due to the applied magnetic field of 500 Oe is insufficient to orient the magnetic moments thus leading to negligible magnetization variation.

The magnetization variation with temperature for two different applied magnetic fields, Figure 8, shows that as the applied magnetic field increases from 500 Oe to 1000 Oe, the magnitude of magnetization increases by nearly five times for both the doping concentrations. This nearly five times magnetization magnitude increase is seen all throughout the temperature range from 4K to 320K. The nearly five times increase of sample magnetization by just two times increase of applied magnetic field clearly corroborates the earlier observation that 500 Oe magnetic field is inadequate to orient the magnetic moments of the samples. But the 1000 Oe magnetic field orients the magnetic moments of the samples.

The Figure 8 shows that for applied magnetic field of 1000 Oe the magnetization value is less for 15% Mn doped Fe_3O_4 compared to 10% Mn doped Fe_3O_4 nanoparticles. This trend is all throughout the measured temperature range. The lower value of magnetization in higher doping of 15% is due to large crystallographic strains in the samples arising due to higher doping as confirmed by the strain values determined from the Hall-Williamson relation in XRD analysis. The larger strains in the crystal structure leads to loss of magnetizatio [34]. Ideally the ZFC and FC curves overlap above the blocking temperature TB. Above TB, the thermal activation kBT (kB is Boltzmann constant and T is sample temperature) overcomes the magnetic anisotropy energy EA making the magnetization direction of each nanoparticles to randomly flip and the nanoparticles become super paramagnetic. The blocking temperature TB values obtained for the present samples from Figure 8 are tabulated in Table 2.

TABLE 2. Blocking temperature T_B of the samples

Applied Magnetic Field (Oe)	Blocking temperature T_B K	
	10% Mn doped Fe_3O_4	15% Mn doped Fe_3O_4
500	232.7	240.9
1000	31.6	34.7

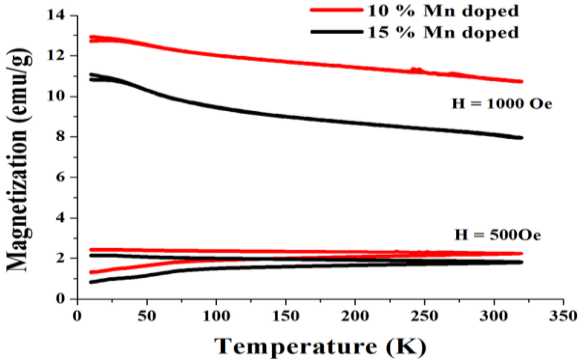

Figure 8. Variation of magnetization as a function of temperature for two different applied magnetic fields of 500 Oe and 1000 Oe, for the synthesized 10% and 15% Mn doped Fe_3O_4 nanoparticles

The table shows that the values of TB are higher for 15% Mn doped Fe_3O_4 nanoparticles compared to 10% Mn doped Fe_3O_4 nanoparticles for both the applied magnetic fields. These results can be substantiated by the Stoner-Wohlfarth theory [35], where energy barrier EA of a single-domain particle is proportional to crystallite volume. The EA serves as an energy barrier to prevent the change in magnetization direction. In the present samples, the XRD analysis showed that the crystallite volume of the 15% Mn doped Fe_3O_4 nanoparticles is greater than the 10% Mn doped Fe_3O_4 nanoparticles. Thus the EA values in case of 15% Mn doped Fe_3O_4 nanoparticles will be greater than the corresponding values of 10% Mn doped Fe_3O_4 nanoparticles. When the thermal activation energy kBT overcomes the magnetic anisotropy energy EA, the nanoparticles magnetization direction moves away from its easy axis and the nanoparticles become super-paramagnetic with the magnetization direction rapidly changing without any preferred orientation. Though there is magnetic ordering in each of the nanoparticles, the conglomeration of the nanoparticles shows paramagnetic behavior. Here the EA values of 15% Mn doped Fe_3O_4 nanoparticles is more compared to 10% Mn doped Fe_3O_4 nanoparticles, thus the corresponding TB will be larger for 15% Mn doped Fe_3O_4 nanoparticles compared to 10% Mn doped Fe_3O_4 nanoparticles.

Table 2 also shows that the values of TB are greater for 500 Oe compared to 1000 Oe for both the doped samples. This can be explained as, with a stronger applied magnetic field, the magnetic moment of the particle easily align to the applied field direction and needing less assistance from thermal agitation. Thus for a stronger applied field the blocking temperature shifts to a lower value [36].

The hysteresis curve between sample magnetization (M) versus the applied magnetic field (H) for 10 and 15% Mn doped Fe_3O_4 nanoparticles measured at 10K and 300K temperatures are shown in Figure 9 (a, b).

The hysteresis curves show that small coercive field (926 Oe for 10% and 1229 Oe for 15%) and remanence magnetization (4.93 emu/g for 10% and 4.14emu/g for 15%) exists in 10K measurements. While, in case of 300K temperature measurements the coercive field and the remanence magnetization is nonexistent. The existence of coercive field and remanence magnetization at 10K states that the sample is ferromagnetic in behavior. The nonexistence of coercive field and remanence magnetization at 300K states super-paramagnetic behavior of the samples. Thus the sample exhibits two varied magnetism at two different temperatures. This can be explained as, the measurement at 300K is above the corresponding TB for both the doped samples, at which the thermal activation energy overcomes the magnetic anisotropy and the magnetization direction of each nanoparticles randomly flip thus nanoparticles become super-paramagnetic. While measurements at 10K are below corresponding TB for both the samples, thus the sample shows ferromagnetic nature .

The comparison of the hysteresis curves, Figure 9, shows that the magnitude values of sample magnetization and its slopes in the applied magnetic field range of 5000 Oe and 50000 Oe are more in case of 10K for both the doped samples. This states that the values of susceptibility are more in case of 10K measurements compared to 300K measurements for both the samples. Also the susceptibility variation with applied magnetic field is more in case of 10K compared to 300K in the applied magnetic field range of 5000 Oe to 50000 Oe. This large value of susceptibility and its greater variation with applied magnetic field states the sample to be ferromagnetic in nature. This ferromagnetic nature of samples at 10K substantiates the earlier result of samples ferromagnetic nature at 10K observed in hysteresis study.

The hysteresis curves analysis shows that the saturation magnetization Ms values in case of 10% Mn doped Fe_3O_4 nanoparticles for temperatures of 10K and 300K are 16.41 and 12.84emu/g, respectively. While the Ms values in case of 15% Mn doped Fe_3O_4 nanoparticles for temperatures of 10K and 300K are 17.49 and 10.38emu/g, respectively.

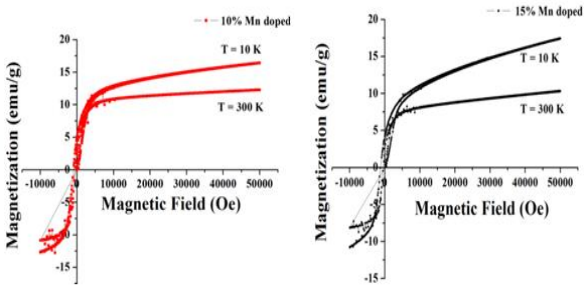

Figure 9. Magnetization (M) versus applied magnetic field (H) for two different temperatures forthe as-synthesized 10% and 15% Mn doped Fe_3O_4 nanoparticles

The data shows that at room temperature of 300K, the Ms value decreases from 12.84emu/g to 10.38emu/g with increase in concentration of Mn dopant from 10% to 15%. This behavior may be due to the removal of Fe cations from the lattice due to doping and leading to imperfect site replacement with the Mn2+ ions. The replacement process results in a disordered structure leading to strain as confirmed from the Hall-Williamson plot in the XRD analysis which significantly decreases the magnetic strength [34]. The imperfect site replacement leads to transition of magnetite to maghemite with its lower sample magnetization values due to the distribution of Fe3+ ions on the tetrahedral and octahedral sites. In case of 10K, the Ms value increases from 16.41emu/g to 17.49emu/g as Mn doping increases from 10% to 15%. This may be due to the low temperature measurements where phonon disorder is least. The other reason is the crystallite size is larger in case of 15% Mn doped Fe_3O_4 nanoparticles compared to 10% Mn doped Fe_3O_4 nanoparticles, thus sample magnetization is more.

CONCLUSION

The 10 and 15% Mn doped Fe_3O_4 nanoparticles were synthesized by simple wet chemical reduction technique. The EDAX analysis of both the Mn doped Fe3O4 nanoparticles confirmed that the synthesized nanoparticles were near stoichiometric and does not contain any impurity. The XRD analysis of the synthesized Mn doped Fe_3O_4 nanoparticles confirmed that both the samples possess cubic unit cell structure. The crystallite size determined from XRD using Scherrer's equation and Hall-Williamson's plot showed that 15% Mn doped Fe_3O_4 nanoparticles have larger crystallite size than the 10% Mn doped Fe_3O_4 nanoparticles. The SEM analysis of the samples showed that the nanoparticles have flower-like patterns on the surfaces. The TEM images showed that the synthesized nanoparticles are spherical in shapes. The optical absorbance analysis of the samples showed that the absorbance edge lies in the wavelength range of 210 nm to 235 nm and absorption is more in case of 10% Mn doped Fe_3O_4 nanoparticles. The peaks of the FTIR absorption spectra could be assigned. The VSM analysis of the samples magnetization as a function of temperature with zero field cooled (ZFC) and field cooling (FC) conditions showed that values of blocking temperature TB are larger for 15% Mn doped Fe_3O_4 nanoparticles compared to 10% Mn doped Fe_3O_4 nanoparticles. The large values of TB in case of 15% Mn doped compared to 10% Mn doped Fe_3O_4 nanoparticles is due to larger crystallite size of 15% Mn doped Fe_3O_4 nanoparticles leading to larger energy barrier EA as per the Stone-Wohlfarth theory. The hysteresis studies showed that both the doped nanoparticles showed ferromagnetic nature at 10K temperature and super-paramagnetic nature at 300K temperature. This is because the temperature of 300K is above corresponding blocking temperature TB and the temperature of 10K is below corresponding blocking temperature TB values.

ACKNOWLEDGEMENT

One of the authors, TJM, is thankful to University Grants Commission (UGC), New Delhi for the award of Maulana Azad National Fellowship (MANF) to carry out this research work. All the authors are thankful to the Sophisticated Instrumentation Centre for Applied Research & Testing (SICART), Vallabh Vidyanagar, Gujarat, India for EDAX, FTIR, TEM and SEM analysis of the samples. The authors are grateful to Dr. Alok Banerjee, UGC-DAE Consortium for Scientific Research (CSR), Indore, India for providing the VSM measurement facility.

REFERENCES

1. S. Kaka, M. Pufall, W. Rippard, T. Silva, S. Russek, and J. Katine, 2005, Mutual phase-locking of microwave spin torque nano-oscillators. Nature. 437, 389-392.
2. H. Lee, M. Huh, Y. Jun, J. Seo, J. Jang, T. Song, S. Kim, J. Cho, G. Yoon, S. Suh, J. Cheon, 2007, Artificially engineered magnetic nanoparticles for ultra-sensitive molecular imaging. J. Nat. Med. 13, 95-99.
3. J. Park, E. Lee, N. Hwang, M. Kang, S. Kim, Y. Hwang, J. Park, H. Noh, J. Kim, J. Park, and T. Hyeon, 2005, One-Nanometer-Scale Size-Controlled Synthesis of Monodisperse Magnetic Iron Oxide Nanoparticles. Angew. Chem., Int. Ed. 44, 2872-2877.
4. C. Yavuz, J. Mayo, W. Yu, A. Prakash, J. Falkner, S. Yean, L. Cong, H. Shipley, A. Kan, M. Tomson, D. Natelson, V. Colvin, 2006, Low-field magnetic separation of monodisperse Fe_3O_4 nanocrystals. Science. 314, 964-967.
5. N. Pinna, S. Grancharov, P. Beato, P. Bonville, M. Antonietti, M. Niederberger, 2005, Magnetite Nanocrystals: Nonaqueous Synthesis. Characterization, and Solubility, Chem. Mater. 17, 3044-3049.
6. Z. Li, L. Wei, M. Gao, H. Lei, 2005, One-Pot Reaction to Synthesize Biocompatible Magnetite Nanoparticles, Adv. Mater. 17, 1001-1005.
7. M. Kim, Y. Chen, Y. Liu, X. Peng, Super-Stable, 2005, High-Quality Fe_3O_4 Dendron–Nanocrystals Dispersible in Both Organic and Aqueous Solutions. Adv. Mater. 17, 1429-1432.
8. H. Ai, C. Flask, B. Weinberg, X. Shuai, D. Pagel, D. Farrell, J. Duerk, J. Gao, 2005. Magnetite-Loaded Polymeric Micelles as Ultrasensitive Magnetic-Resonance Probes. Adv. Mater. 17, 1949-1952.

9. G. Kurlyandskaya, D. Portnov, I. Beketov, A. Larrañaga, A. Safronov, I. Orue, A. Medvedev, A. Chlenova, M. Sanchez-Ilarduya, A. Martinez-Amesti , A. Svalov, 2016 Nanostructured materials for magnetic biosensing. Biochimica et Biophysica Acta (http://dx.doi.org/10.1016/j.bbagen.2016.12.003).
10. A. Safronov, I. Beketov , I. Tyukova, A. Medvedev, O. Samatov, A. Murzakaev, 2015. Magnetic nanoparticles for biophysical applications synthesized by high-power physical dispersion. Journal of Magnetism andMagneticMaterials. 383, 281–287.
11. F. Owens, 2003, Ferromagnetic resonance of magnetic field oriented Fe_3O_4 nanoparticles in frozen ferrofluids. Journal of Physics and Chemistry of Solids. 64, 2289–2292.
12. T. Malek, S. Chaki, J. Tailor and M. Deshpande, 2016, Thermal Decomposition Study of Mn doped Fe_3O_4 Nanoparticles. AIP Conf. Proc. 1728, 020390-5 pages.
13. J. Hastings and L. Corliss, 1956, Neutron Diffraction Study of Manganese Ferrite. Phys. Rev. 104, 328-331.
14. M. Ishikawa, H. Tanaka, T. Kawai, 2006, Preparation of highly conductive Mn-doped Fe3O4 thin films with spin polarization at room temperature using a pulsed-laser deposition technique. Appl. Phys. Lett. 86, 222504-4 pages.
15. D. Tripathy, O. Adeyeye, B. Boothroyd, N. 2007, Piramanayagam, Magnetic and transport properties of Co-doped Fe3O4 films. J.Appl. Phys. 101, 013904-7 pages.
16. Z. Jing, S. Wu, 2006, Synthesis, characterization and gas sensing properties of undoped and Co-doped γ-Fe_2O_3-based gas sensors. Mater. Lett. 60, 952-956.
17. G. Neri, A. Bonavita, C. Milone, S. Galvagno, 2003, Role of the Au oxidation state in the CO sensing mechanism of Au/iron oxide-based gas sensors. Sens. Actuators B. 93, 402-408.
18. L. Jianjun, Y. Hongming, L. Guodong, L. Yanju, L. Jinsong, 2010, Cation distribution dependence of magnetic properties of sol–gel prepared $MnFe_2O_4$ spinel ferrite nanoparticles. J.Magn. Magn. Mater. 322, 3396-3400.
19. J. Amighian, M. Mozaffari, B. Nasr, 2006, Preparation of nano-sized manganese ferrite (MnFe2O4) via co-precipitation method. Phys. Status Solidi C. 3, 3188-3192.
20. C. Liu, B. Zou, A. Rondinone, Z. Zhang, Counterion. 2000, Effect in Acid Synthesis of Mesoporous Silica Materials. J. Phys. Chem. B. 104, 7885-7894.
21. G. Kurlyandskaya, S. Bhagat, S. Jacobo, J. Aphesteguy, N. Schegoleva, 2011, Microwave resonant and zero-field absorption study of pure and doped ferrite nanoparticles. Journal of Physics and Chemistry of Solids. 72, 276–285.
22. E. Kima, H. Leea, B. Kwakb, B. Kimc, 2005, Synthesis of ferrofluid with magnetic nanoparticles bysonochemical method for MRI contrast agent. Journal of Magnetism and Magnetic Materials. 289, 328–330.
23. D. Zhang, X. Zhang, X. Ni, J. Song, H. Zheng, 2006. Low-temperature fabrication of MnFe2O4 octahedrons: Magnetic and electrochemical properties. Chem. Phys. Lett. 426, 120-123.
24. S. Chaki, T. Malek, M. Chaudhary, J. Tailor, M. Deshpande, 2015. Magnetite Fe_3O_4 nanoparticles synthesis by wet chemical reduction and their characterization. Adv. Nat. Sci: Nanosci. Nanotechnol. 6, 035009-6.
25. S. Chaki, M. Deshpande, M. Chaudhary, K. Mahato, 2013. Synthesis and Characterization of Tin Monosulphide Nanoparticles. Adv. Sci. Eng. Med. 5, 285-290.
26. M. Elango, K. Gopalakrishnan, S. Vairam, M. 2012. Thamilselcan, Strutural, optical and magnetic studies on non-acqueous synthesized Cd: Mn nanoparticle. J. Alloys Compd. 538, 48-55.
27. Y. Vodyanitskii, E. Morgun, L. Obydenova, K. Rumyantseva, N. Chapygina, 2009. Geochemistry of Magnetite and Maghemite in Soils in European Russia. Geochem. Int. 47, 297-310.
28. S. Rana, J. Philip, B. Raj, 2010. Micelle based synthesis of cobalt ferrite nanoparticles and its characterization using Fourier Transform Infrared Transmission Spectrometry and Thermogravimetry. Materials Chemistry and Physics. 124, 264-269.
29. X. Liang, X. Wang, J. Zhuang, Y. Chen, D. Wang, Y. Li, 2006. Synthesis of Nearly Monodisperse Iron Oxide and Oxyhydroxide Nanocrystals. Advanced Functional Materials. 16, 1805-1813.
30. L. Rebodos, J. Vikesland, 2010. Effects of Oxidation on the Magnetization of Nanoparticulate Magnetite. Langmuir. 26, 16745-16753.
31. K. Kim, S. Kim, Y. Choa, H. Kim, 2007. Formation and Surface Modification of Fe_3O_4 Nanoparticles by Co-precipitation and Sol-gel Method. J. Ind. Eng. Chem. 13, 1137-1141.
32. E. McCafferty, 2010. Relationship between the isoelectric point (pHpzc) and the potential of zero charge (Epzc) for passive metals. Electrochim. Acta. 55, 1630–1637.
33. C. Caizer, V. Tura, 2006. Magnetic relaxation/stability of Co ferrite nanoparticles embedded in amorphous silica particles. J. Magn. Magn. Mater. 301, 513-520.
34. C. Warner, W. Chouyyok, K. Mackie, D. Neiber, L. Saraf, T. Droubay, M. Warner, R. Addleman, 2012. Manganese doping of Magnetic Iron Oxide nanoparticles: Tailoring surface reactivity for a regenerable heavy metal sorbent. Langmiur. 28, 3931-3937.
35. E. C. Stoner, E. P. Wohlfarth, 1948. A mechanism of magnetic hysteresis in heterogeneous alloys. Phil. Trans. R. Soc. A. 240, 599-642.
36. Christy R. Vestal, Z John Zhang, 2004. Magnetic spinel ferrite nanoparticles from microemulsions. Int. J. Nanotechnology. 1, 240 – 263.

Persian Abstract

DOI: 10.5829/ijee.2018.09.02.xx

چکیده

اثر دوپینگ Mn بر ذرات اسپینل نانوکریستال Fe_3O_4 مورد بررسی قرار گرفته است. دو غلظت دوگانه ۱۰ و ۱۵ درصد Mn مورد استفاده قرار گرفتند. سنتز نانوذرات توسط روش کاهش شیمیایی مرطوب انجام شد. تجزیه و تحلیل پراکنده انرژی اشعه ایکس، استئوکیومتری نمونه ها را تایید کرد. برای تعیین ساختار بلوری و اندازه ذرات نانوذرات سنتز شده از روش پراش اشعه X استفاده شد. میکروسکوپ الکترونی نشان داد که هر دو سطوح نانوذرات سنتزی دارای الگوهای گل مانند هستند و ذرات کروی هستند. مطالعه جذب نوری نشان داد که جذب بیشتر در مورد ۱۰٪ Mn doped در مقایسه با ۱۵٪ Mn doped Fe_3O_4 نانوذرات بیشتر است. طیف سنجی مادون قرمز تبدیل فوریه نشان داد که هر دو نمونه دارای نوارهای خاصی هستند. تغییرات مغناطیسی با دمایی با خنک کننده صفر و شرایط خنک کننده میدان برای دو میدان مغناطیسی مختلف ۵۰۰ Oe و ۱۰۰۰ Oe و همچنین مطالعه هیسترزی با روش مغناطیس سنجی نمونه ارتعاشی انجام شد. نتایج به دست آمده در جزئیات مورد بحث قرار می گیرد.